

# One-pot polymerization, surface grafting, and processing of waterborne polyurethane-cellulose nanocrystal nanocomposites

Xiaodong Cao,<sup>†</sup> Youssef Habibi and Lucian A. Lucia\*

Received 28th May 2009, Accepted 28th July 2009

First published as an Advance Article on the web 24th August 2009

DOI: 10.1039/b910517d

A series of new waterborne polyurethane (WPU)/cellulose nanocrystal (CN) composites have been successfully synthesized *via in situ* polymerization. The conditions were optimized to induce the grafting of part of the pre-synthesized WPU chains on the surface of cellulose nanocrystals (CNs) and the corresponding nanocomposites were processed by casting and evaporation. The morphology, structural, thermal, and mechanical properties of the resulting nanocomposite films were evaluated by scanning electron microscopy, wide-angle X-ray diffraction, differential scanning calorimetry, dynamic mechanical analysis, and tensile tests. The success of the grafting was substantiated by Fourier transform infrared spectroscopy, X-ray photoelectron spectroscopy and differential scanning calorimetry. Thus, it was demonstrated that the grafted WPU chains formed crystalline domains on the surface of CNs which expedited the crystallization of the polycaprolactone (PCL) soft segment domains in the WPU/CN nanocomposites. This co-crystallization phenomenon induced the formation of a co-continuous phase between the matrix and filler which significantly enhanced the interfacial adhesion and consequently contributed to an improvement in the thermal stability and mechanical strength of the nanocomposites. Although the ductility of the final nanocomposites was slightly reduced, in the CN content range from 0 to 10 wt-%, the Young's modulus and strength were significantly improved as shown by the change from 1.7 to 107.4 MPa and 4.4 to 9.7 MPa, respectively.

## Introduction

The introduction of reinforcing nanoparticles/materials into a continuous polymer phase to form nanocomposites has attracted a great deal of attention recently because it can provide significant improvements in mechanical properties at very low volume fractions of the reinforcing phase. Typical reinforcement phases have included clay,<sup>1–4</sup> hydroxyapatite,<sup>5</sup> and multi-walled carbon nanotubes;<sup>6–8</sup> more recently, cellulose nanocrystals (CNs). CNs have received increasing attention as reinforcing materials in nanocomposites due to their low cost, high availability, renewability, nanoscale dimensions, large surface area, unique morphology, ease of chemical modification, low density, and good mechanical response to stress.<sup>9,10</sup> For example, the probability of CNs contributing to significant enhancements in the mechanical properties of a co-CN/polymer composite is high because the theoretical value of the Young's modulus of pure crystalline cellulose domains is estimated to be 150 GPa.<sup>11,12</sup> Since the first report of using CNs from *tunicin* (animal cellulose) as a reinforcing phase in a matrix of latex by Favier *et al.*,<sup>13</sup> CNs from various sources such as cotton,<sup>14</sup> tunicate,<sup>15–18</sup> algae,<sup>19,20</sup> bacteria,<sup>21,22</sup> ramie,<sup>23–25</sup> and wood<sup>26,27</sup> have been widely investigated for the preparation of high performance composite materials based on a wide range of polymers matrices.

Polyurethane (PU) is a polymer of use for a variety of high end medical, industrial, and technological applications. It has found

wide spread application in a range of commodity products such as elastomers, foams, paints, and adhesives. PU is the general name for a family of synthetic co-polymers that contain the urethane moiety in their chemical repeat structure. They comprise a large family of polymeric materials with a wide diversity of chemical compositions and properties. Such diversity originates from the tunable chemistry of the polyurethanes, *i.e.*, the chemical composition of polyurethanes can be tuned by choosing different raw materials and processing conditions to accommodate a specific requirement.<sup>28</sup>

Yet, in spite of the attractive qualities mentioned above, conventional polyurethane products usually contain a significant amount of organic solvents and occasionally free isocyanate monomers.<sup>29</sup> Therefore, they have been gradually replaced by waterborne polyurethanes (WPU) because of increasing concerns about environmental pollution, health, and safety risks.<sup>30–33</sup> Additionally, WPU possess several of the attractive advantages associated with conventional organic solvent-borne PU such as low viscosity at high molecular weight, nontoxicity, and good applicability without the accompanying liabilities mentioned above.<sup>34</sup>

In our previous work,<sup>35</sup> we prepared a series of nanocomposite films with an aqueous suspension of CNs as the filler and a polycaprolactone (PCL)-based WPU as the matrix by simple blending in water. The nanocomposite films showed a significant increase in Young's modulus and tensile strength from 0.51 to 344 MPa and 4.27 to 14.86 MPa, respectively, with increasing filler content from 0 to 30 wt-%. However, these gains were obtained at the expense of reduced elongation at break from 1086% to 186%, which corresponds to what most previous

Department of Forest Biomaterials, North Carolina State University, Campus Box 8005, Raleigh, NC 27695-8005, USA

<sup>†</sup> Present Address: Biomedical Engineering Institute, South China University of Technology, Guangzhou, Guangdong, 510640, China.

studies have found when fabricating polymer composites that employ CNs as the filler. As is already known, a high content loading of hydrophilic nanoparticles within a hydrophobic polymer matrix will almost certainly result in an aggregation of the particles, resulting in a failed mechanical response of the composites. Therefore, to prepare high performance nanocomposite materials with a hydrophobic polymer matrix and a hydrophilic CN filler, the major issues to address are adequate dispersion and developing strong interfacial adhesion between the matrix and the filler. Obviously, the most ideal and effective way is through covalent attachment of the polymer to the stiff surface of CNs by taking advantage of the abundant hydroxyl groups on the surface of CNs.<sup>24,36,37</sup>

In this research, we report the novel preparation of WPU/CN nanocomposites *via* a one-pot synthesis reaction between the exposed hydroxyl functionalities on the CN surfaces and isocyanate on the ends of the WPU prepolymer, and further processing of the resulting nanocomposites by the casting-evaporation technique. The morphology, structural, thermal and mechanical properties of the resulting nanocomposite films were investigated by Fourier transform-infrared spectroscopy (FT-IR), X-ray photoelectron spectroscopy (XPS), scanning electron microscopy (SEM), wide-angle X-ray diffraction (WAXD), differential scanning calorimetry (DSC), thermogravimetric analysis (TGA), dynamic mechanical analysis (DMA), and mechanical properties measurements.

## Experimental

### Materials

Cottonseed linter was supplied by Hubei Chemical Fiber Manufacture, China. Polycaprolactone diol ( $M_n = 1250$ ), isophorone diisocyanate (IPDI), dimethylol propionic acid (DMPA), triethylamine (TEA), acetone, N,N-dimethylformamide (DMF), and concentrated sulfuric acid (98%) were purchased from Sigma-Aldrich Corporation and used as received without further purification.

### Cellulose nanocrystals preparation

The cottonseed linter pulp (30 g) was cut into small pieces, and then mixed with sulfuric acid aqueous solution (250 mL, 64 wt-%) under vigorous stirring at 60 °C for 2 h. Subsequently, the suspension was washed with water by successive centrifugation and dialyzed against deionized water until the pH of the suspension was neutral. The solvent exchange of the obtained suspension was done from water to acetone, then from acetone to DMF by several successive centrifugation steps at 12,000 rpm and 10 °C for 20 min. Finally, a stable suspension in DMF with a solid content of 5.0 wt-% was obtained through 10 min ultrasonic treatment, which then was stored before use.

### Preparation of WPU/CNs nanocomposite films

Polycaprolactone diol (12.0 g) and DMPA (0.8 g) were introduced into a four-necked flask equipped with mechanical stirrer, condenser and thermometer. The mixture was heated to 80 °C until the polycaprolactone diol melted completely; then IPDI (4.8 g) was added dropwise, and the reaction was carried out

under a dry nitrogen atmosphere for 2 h. Subsequently, the desired amount of CNs suspended in DMF was added and the reaction was allowed to continue to react for another two hours. After removing DMF by vacuum between 60 to 80 °C, approximately 50 mL of acetone was poured into the flask to reduce the viscosity of the pre-polymer and the solution was cooled down to 60 °C. After neutralization of the carboxylic groups of DMPA with TEA (0.6 g) for 30 min, the product was dispersed in distilled water under vigorous stirring. After stirring at room temperature overnight, the suspension volume was reduced to a WPU solid content of 25 wt-% by rotary vacuum evaporation at 30 °C. The suspension was finally cast in Teflon Petri dishes and dried in an oven at 40 °C for 10 h and thus became a film. By changing the content of CN over a range from 0, 2, 4, 6, 8, and 10 wt-%, a series of nanocomposite films with a thickness of approximately 0.5 mm were obtained, and coded as WPU, WPU/CN-2, WPU/CN-4, WPU/CN-6, WPU/CN-8, and WPU/CN-10, respectively. The resulting films were stored at room temperature in a desiccator containing P<sub>2</sub>O<sub>5</sub> with 0% relative humidity (RH). In order to control the success of the grafting and to determine the amount of grafted WPU, the resulting films were subjected to Soxhlet extraction with acetone for 48 h, and the residual products were weighed and further characterized.

### Characterization

**Fourier transform infrared analyses.** FTIR spectroscopy was performed on a Nicolet FTIR spectrometer (Perkin-Elmer-FTIR spectrophotometer, Nicolet Nexus 470) at room temperature. Powder of unmodified-CN or modified CNs (obtained after Soxhlet extraction) were ground with KBr and pressed into pellets. The data were collected over 64 scans with a resolution of 4 cm<sup>-1</sup>.

**X-Ray photoelectron spectroscopy (XPS).** XPS measurements were performed on the dried pellets of powder CNs before and after the WPU grafting with a Kratos AXIS Ultra photoelectron spectrometer. Pellets from dried powder were prepared and washed with chloroform to remove contaminants and then kept in a vacuum oven for at few hours at 40 °C prior to analysis. The XPS experiments were conducted at room temperature with a base pressure of  $1 \times 10^{-9}$  mbar. The monochromatic Al K $\alpha$  X-ray source was operated at 300 W (15 kV, 20 mA). The low-resolution survey scans were taken with a 1 eV step and 80 eV analyzer pass energy; high-resolution spectra were taken with a 0.1 eV step and 20 eV analyzer pass energy. Quantitative XPS analyses were performed with the Kratos Vision software (version 2.1.2). The atomic concentrations were calculated from the photoelectron peak areas by using Gaussian-Lorentzian deconvolution. The carbon 1s spectra were resolved into different contributions of bonded carbon, namely carbon without oxygen bond (C-C and C-Hx), carbon with one oxygen bond C-O, carbon with two oxygen bonds O-C-O, and carbon with three oxygen bonds O-C=O. The chemical shifts were taken from the literature and the spectra were charge corrected by setting the carbon without oxygen bond contribution in the C1s emission at 285.0 eV.<sup>38</sup>

**Field emission scanning electron microscopy.** Cross-section micrographs of nanocomposite films were obtained with a field

emission scanning electron microscope (FESEM) (JEOL JSM-6400F, Japan) at 5 kV. The specimens were frozen in liquid nitrogen, snapped, and then coated with an approximately 100 angstrom of gold/palladium (60/40) before observation.

**Transmission electron microscopy.** Drops of aqueous dispersions of unmodified cellulose nanocrystals (0.01% w/v) were deposited on carbon-coated electron microscope grids (Protochips Inc.), negatively stained with uranyl acetate and allowed to dry. The samples were analyzed with a Hitachi HF-2000 transmission electron microscope (TEM) operated at an accelerating voltage of 80 kV.

**Wide-angle X-ray diffraction (WAXD).** Wide-angle X-ray diffraction patterns were recorded on an X-ray diffractometer with a Highstar area detector (Bruker D-5000), using Cu K $\alpha$  radiation ( $\lambda = 15.405$  nm) at 40 kV and 30 mA. The  $2\theta$  ranged from 5 to 40° with a  $2\theta$  step of 0.05°.

**Differential scanning calorimetry.** DSC measurements were carried out for unmodified CNs, modified CNs (obtained after Soxhlet extraction), or nanocomposite films on a thermal analyzer (TA instrument DSC Q100) under a nitrogen atmosphere. Each sample (10 mg) was heated from -90 to 100 °C at a heating rate of 10 °C/min. The glass transition temperature ( $T_g$ ) was determined from the midpoint temperature of the overall heat capacity change, while the melting temperature ( $T_m$ ) was taken as the peak temperature of the melting endotherm. The degree of crystallinity in the PCL soft segments domain was calculated according to the melting peak area of the DSC curves, assuming that a perfect PCL crystallite has a melting enthalpy of 0.14 kJ/g.<sup>39</sup>

**Thermogravimetric analysis.** A thermogravimeter (TA instrument TGA Q500) was used to measure the weight loss of the WPU and WPU/CN nanocomposite films as well as CNs under nitrogen atmosphere. The samples were heated from 30 °C up to 600 °C at a heating rate of 10 °C/min. Generally, approximately 10 mg samples were used for each thermogravimetric analysis.

#### Mechanical properties measurements

(1) *Dynamic mechanical analysis.* The dynamic mechanical behavior of the nanocomposite films was determined using a dynamic mechanical analyzer (TA instrument DMA Q800) with tensile mode at 1 Hz and a heating rate of 5 °C/min in the temperature range of -100 to 100 °C. The samples were prepared by cutting 6 mm wide strips from the films.

(2) *Tensile measurements.* The mechanical behavior at large deformations for the nanocomposites was analyzed with an Instron Universal Testing Machine (model-4411) at room temperature with gauge length of 3 cm and crosshead speed of 50 mm min<sup>-1</sup>. An average value of at least five replicates for each sample was taken.

## Results and discussion

### Preparation of WPU/CN nanocomposites

The rod-like CNs produced from sulfuric acid hydrolysis of cottonseed linters were characterized by TEM as shown in Fig. 1.

The width varied from 10 to 20 nm whereas the length varied from 70 to 150 nm. These dimensions agreed well with the literature values reported for CNs produced from the same cellulosic material under similar conditions.<sup>40</sup> However, a wide distribution of CNs size, especially the length, is inevitable owing to the diffusion-controlled nature of the acid hydrolysis.

Different levels of CNs were introduced to a bulk WPU polymerization to induce simultaneous grafting onto their surfaces. After the reaction, the resulting material was one-pot processed by a casting-evaporation technique. In order to control the success of the grafting and to determine the amount of WPU polymer that had been grafted, the resulting composites were subjected to Soxhlet extraction with acetone for 48 h. After drying, the residues were weighed and analyzed. Table 1 shows the mass of the residual product after extraction and the calculated amount of grafted WPU based on the initial mass of CNs introduced into the bulk reaction. It was found that the amount of grafted WPU varied from 45 to 57% on a weight basis. In general, the linear polyurethanes are soluble in acetone and thus only WPU covalently linked to CNs will remain after complete Soxhlet extraction by acetone. Based on the above results, it can be easily concluded that part of the WPU pre-polymer molecules terminated with isocyanate groups have reacted effectively with the hydroxyl groups on the CNs.

These residues were also analyzed by FT-IR; the spectrum of WPU/CN-10 is given as an example in Fig. 2. As a comparison, control spectra of unmodified CNs and WPU are also reported. By comparison to CNs, two new absorbance bands localized at 1732 cm<sup>-1</sup> and 1557 cm<sup>-1</sup> were found, which also can be observed in the spectrum of WPU and are assigned to the stretching vibration of the C=O groups and the bending of the N-H bond, respectively. The improved strength of the peaks located at 2903 cm<sup>-1</sup> and 2861 cm<sup>-1</sup>, which correspond to the alkane C-H asymmetric and symmetric stretching vibrations, indicates that there are more -CH<sub>2</sub>- in the residues than in the CNs. This demonstrates the presence of WPU molecules in the residue after the extraction and confirms the success of the grafting.

The presence of WPU polymer was also confirmed by XPS measurements. X-Ray photoelectron spectra (XPS) were determined for the main elements and for the carbon-based bonds in order to evaluate the chemical composition of the substrates, especially the occurrence of WPU presence before and after reaction. Low resolution spectra of both unmodified CNs show that carbon and oxygen atoms are the main components, while in

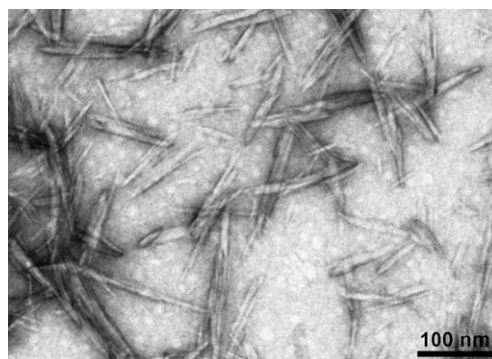
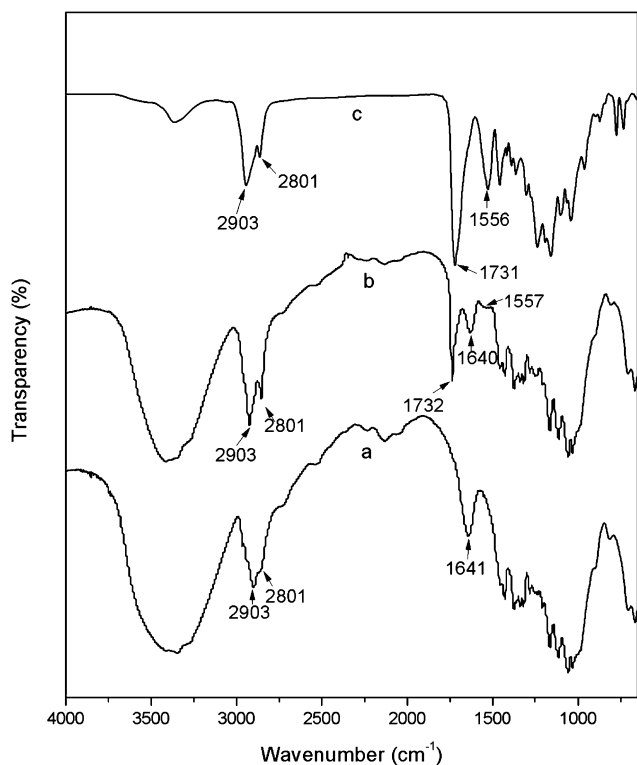


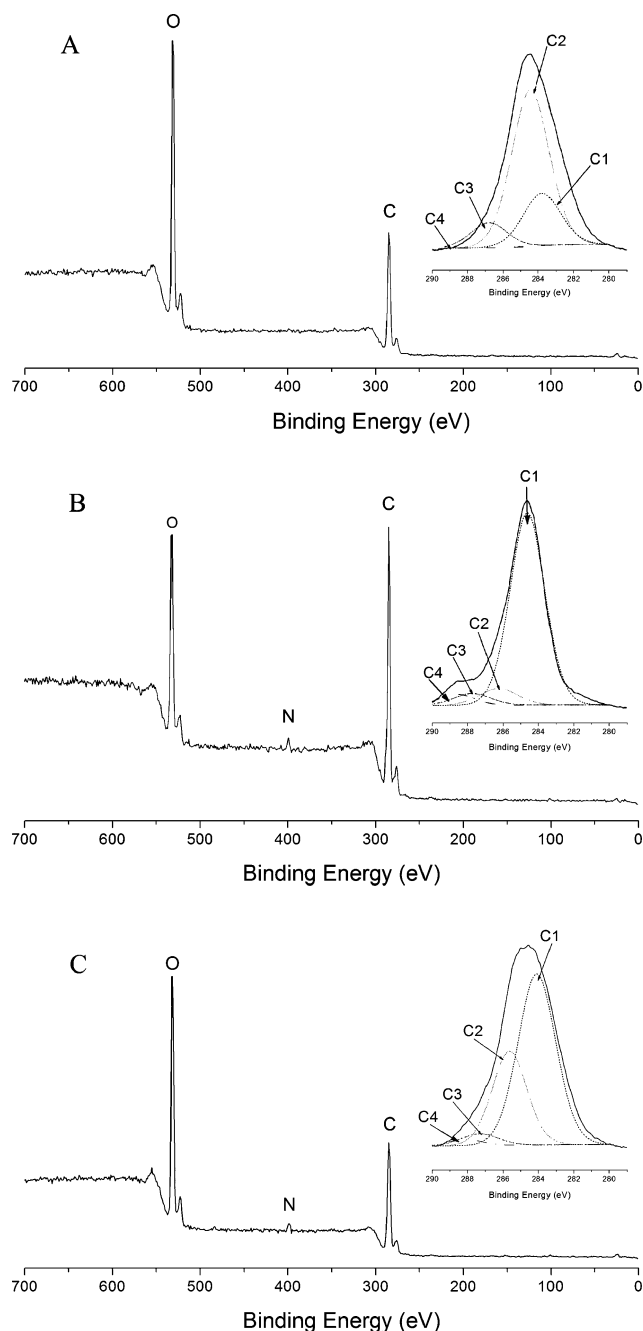
Fig. 1 A TEM image of the CNs hydrolyzed from cotton linter.

**Table 1** Compositions of WPU/CN nanocomposites before and after Soxhlet extraction

Samples	Initial mass (g)	Mass of CNs in the sample (g)	Mass of residue (g)	%-wt WPU in the residue
WPU	2.25	0	0	0
WPU/CN-2	5.80	0.12	0.24	51.5%
WPU/CN-4	2.71	0.11	0.20	45.7%
WPU/CN-6	2.78	0.17	0.33	49.4%
WPU/CN-8	4.19	0.34	0.78	57.0%
WPU/CN-10	5.82	0.58	1.24	53.1%

**Fig. 2** FTIR spectra of (a) unmodified CNs, (b) the residue obtained from WPU/CN-10 nanocomposites after Soxhlet extraction with acetone for 48 h, and (c) neat WPU.

modified cellulosic substrates (WPU/CN-2 and WPU/CN-10) given as example) nitrogen is also present (Fig. 3). In the high-resolution carbon spectra (inside Fig. 3A), the carbon signal can be resolved into several component peaks, which reflect the local environments of the carbon atoms (C–C and C–H or C–O or O–C–O or O–C=O). In all samples, the four component peaks are therefore categorized by the kind of bonds where C is involved in WPU and/or cellulose structures. The relative amounts of each carbon type in the samples were determined before and after grafting. The XPS spectra of both unmodified and WPU-grafted CNs exhibit contributions of each type of carbon atoms, but at different proportions. The ratio of carbon atoms with two bonds to oxygen relative to carbon atoms with one bond to oxygen (O–C–O/C–O) was found to be 0.19 which is very close to the theoretical value of 0.2 expected from the formula of pure cellulose (C<sub>6</sub>O<sub>5</sub>H<sub>9</sub>)<sub>n</sub>. The presence of carbon with three bonds to oxygen in the unmodified CNs can be explained by the presence of carboxylic groups resulting from the

**Fig. 3** XPS wide scans from cellulose nanocrystals before (A) and after the WPU grafting reaction and Soxhlet extraction (B, WPU/CN-2 and C, WPU/CN-10). Insets: high resolution carbon spectra: C1: C–C (C–H<sub>x</sub>), 285.0 eV; C2: C–O, 286.5 eV; C3: O–C–O, 288.0 eV; C4: O–C=O, 289.0 eV.

oxidation of the reducing end groups of cellulose. Nevertheless, the presence of carbon without oxygen bonds can be explained only by the presence of contaminants because pure cellulose does not possess a carbon atom without an oxygen bond.

After the WPU grafting reaction, the proportion of each carbon atom significantly varied, which was especially true for the proportions of carbon atoms without oxygen linkages and carbon atoms with three oxygen bonds (inside Fig. 3B and C). The presence of WPU polymers on the surface must be invoked to explain the high proportions of these types of carbon atoms. In addition, an additional peak attributed to nitrogen appears after the WPU grafting reaction which can only be explained by the presence of isocyanate groups. These results further confirm the presence of WPU and demonstrate the efficiency of the grafting onto CNs.

These results are confirmed further by DSC analyses. The obtained residues were investigated by DSC; Fig. 4 illustrates the thermograms of unmodified CNs and, as an example, the residues obtained from nanocomposite formulations WPU/CN-2 and WPU/CN-8. Surprisingly, the grafted CNs that remain after Soxhlet extraction display a low magnitude, but well defined melting endotherm around 45 to 47 °C, which was not observed for the original nanocrystals. It can be logically attributed to the melting of PCL soft segment from grafted WPU polymeric chains that likely form a crystalline structure at the surface of the nanocrystals. It can be rationalized by the appearance of grafted WPU chains on the surface of CNs that adopt a crystalline brush-like structure that extends outward from the nanocrystals' surface. Each cellulose nanocrystal is capable of binding multiple WPU pre-polymer molecules in a well ordered shell-like structure on the surface that *de facto* has a restricted mobility and consequently is able to crystallize. Similar behavior of extensive crystallization of stearate moieties grafted onto starch nanocrystal surfaces, forming crystalline hydrophobic shells around the hydrophilic nanoparticles, has already been reported.<sup>41</sup> Additionally, surface crystallization of grafted PCL chains onto the surface of CNs has already been reported in which it was found

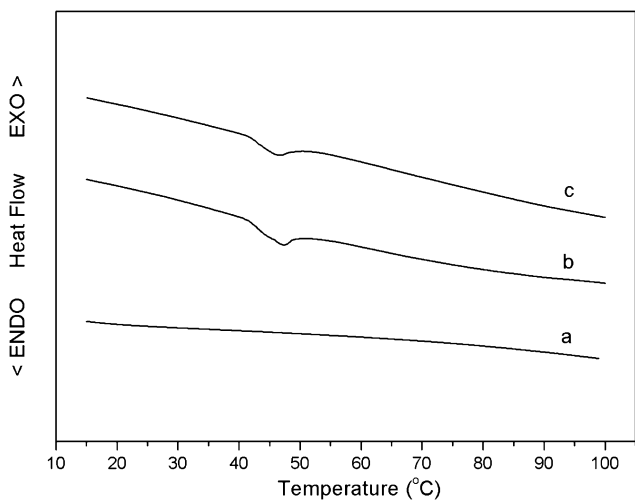


**Fig. 4** The DSC thermograms of (a) unmodified CNs and the residues obtained from (b) WPU/CN-2 and (c) WPU/CN-8 nanocomposites after Soxhlet extraction with acetone for 48 h.

that it gave rise to a co-continuous phase in the nanocomposite as a result of the interfacial adhesion between the filler and the matrix.<sup>24,25</sup> It was further demonstrated that this improved adhesion significantly enhanced the thermomechanical properties of the resulting nanocomposites.

### Morphology and structure of WPU/CN nanocomposites

Fig. 5 illustrates the FESEM images of a cross-section of the unfilled WPU matrix and nanocomposite films filled with 2, 6, and 10 wt-% of CNs, respectively. Compared to the micrograph of unfilled WPU, the morphology of the CNs in the WPU matrix can easily be identified. The CNs appear as white dots, whose concentration on the fracture surface of the nanocomposites increased directly with an increase of the filler loading. Furthermore, a uniform distribution of CNs in the WPU matrix was observed in all of the nanocomposites, which demonstrated that good compatibility between the fillers and matrix was achieved. Improved compatibility between WPU and CNs can be ascribed to the covalent bonding between CNs and WPU and the co-crystallization event that can occur between the grafted WPU chains and WPU from the matrix. Such uniform distribution of the fillers in the matrix is anticipated to play an important role in the improvement of the performance of the resulting nanocomposite films.

The WAXD of the nanocomposites was studied as a function of the CN content, and the corresponding diffractograms are shown in Fig. 6. CNs display four well-defined diffraction peaks at 14.7°, 16.5°, 22.7°, and 34.5°, which are typical of cellulose I.<sup>42,43</sup> For the neat WPU, there is only a broad diffraction hump at  $2\theta = 19^\circ$  indicating the amorphous nature of the film. It can be explained by the fact that polyurethane that has been prepared with PCL having soft-segments with a molecular weight lower than 2000 usually shows no crystallinity.<sup>43,44</sup> Interestingly, new diffraction peaks appear in the diffractograms when CNs are added into the WPU matrix. By comparison with the patterns of WPU and CNs, the two new diffraction peaks at  $2\theta = 20.8^\circ$  and

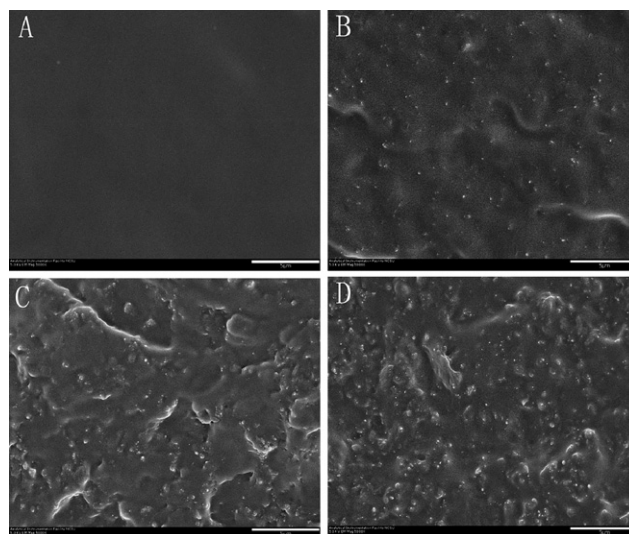


**Fig. 5** FESEM images of the WPU/CNs nanocomposites with different CNs content: (A) 0, (B) 2, (C) 6, and (D) 10 wt-% (scale bar = 5  $\mu$ m).

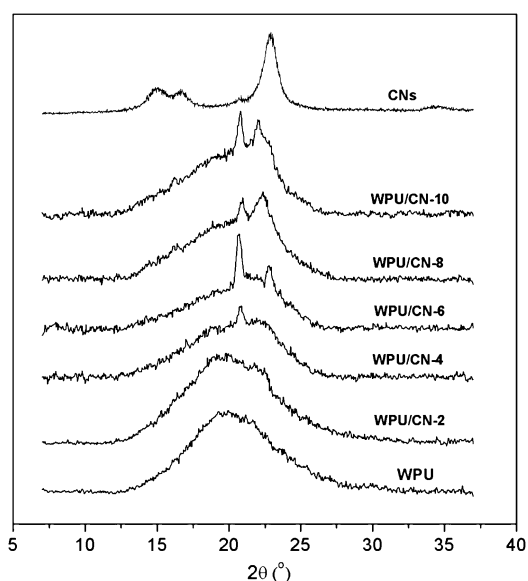


Fig. 6 WAXD patterns of CNs, WPU and WPU/CN nanocomposites with different CNs loading.

22.8° are easily evidenced. These peaks can be assigned to crystalline PCL soft segments of WPU because PCL is a type of semi-crystalline thermoplastic polymer with characteristic peaks at approximately 21.5°, 22°, and 23.5°. This unusual behavior was not evidenced when unmodified CNs were blended with the same WPU matrix<sup>35</sup> because the system is not interfacially compatible, so nucleation on the CNs is not permitted. However, the presence of the grafted WPU chains on the surface of CNs provided a crystalline environment as already demonstrated (by DSC) which we conjecture will further induce the crystallization of the WPU polymeric chains from the matrix surrounding the CNs.

#### Thermal properties of WPU/CN nanocomposites

Fig. 7 shows the TGA curves for the CNs, WPU, and WPU/CN nanocomposites having various loading levels of CNs. The thermogram of unmodified CNs showed the typical degradation profile of CNs possessing sulfate groups that arise from fiber hydrolysis with sulfuric acid.<sup>46</sup> The main cellulose degradation occurs between 200 °C and 300 °C due to its depolymerization, dehydration, and decomposition of glycosyl units followed by the formation of a char. The small shoulder above 325 °C can be ascribed to the oxidation and breakdown of the char to lower molecular weight gaseous products. However, no separate degradation stage of the CNs can be found in any TGA curves of the WPU/CN nanocomposites regardless of the CNs loading level, which indicates that CNs have been completely covered by the WPU molecules through the reaction between CNs and WPU pre-polymer. Interestingly, the WPU/CN nanocomposites have a maximum degradation temperature ( $T_{max}$ ) at about 400 °C which is much higher than the degradation temperature of pure WPU (337 °C). This significant enhancement of thermal resistance by the presence of CNs can be attributed to the formation of a confined structure in the WPU/CN nanocomposites. Although the  $T_{max}$  of WPU/CN nanocomposites is higher than that of WPU, they start to decompose at the same

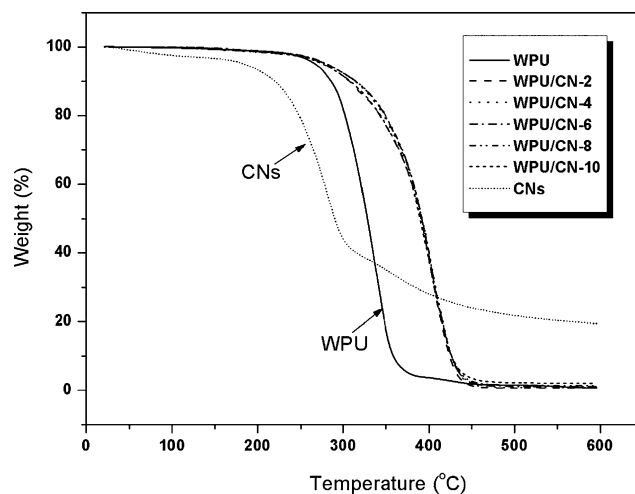


Fig. 7 TGA curves of CNs, WPU and WPU/CN nanocomposites with different CNs loading.

temperature of about 250 °C probably because of the low amount of CN loaded (maximum of 10%). This is reflected by the thermal stability (similar  $T_{max}$ ) of all WPU/CN nanocomposites at low CN loading levels of 2 to 10 wt-%.

To further understand the structure and interactions between the two components, DSC studies of the unfilled and filled nanocomposites were conducted. Fig. 8 shows the DSC thermograms of WPU matrix and nanocomposites reinforced with varying amounts of CNs, and the corresponding data are presented in Table 2. In all curves, a specific heat increment is observed at around -45 °C which corresponds to the glass-rubber transition of the soft segments of the WPU matrix. As can be observed, the  $T_g$  increased as the amount of CN increased and it varied from -47.97 °C for neat WPU to approximately

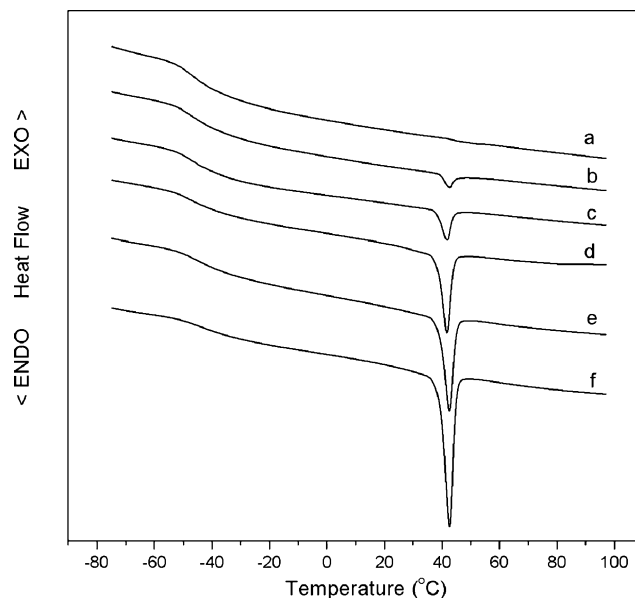


Fig. 8 DSC thermograms of WPU and WPU/CN nanocomposites with different CNs loading: (a) WPU, (b) WPU/CN-2, (c) WPU/CN-4, (d) WPU/CN-6, (e) WPU/CN-8, (f) WPU/CN-10.

–43.47 °C for WPU with a 10% CNs loading. The restricted mobility of WPU chains neighboring CNs that is due to the co-crystallization event with those grafted on the surface might be the origin of the shift of  $T_g$  towards higher temperature. Also, it is hypothesized that this co-crystallization could also enhance the interactions between soft and hard segments and therefore limit the microphase separation in WPU which could also indirectly result in an increase of  $T_g$  of the soft segments of WPU.

Interestingly, an endothermic peak, assigned to the melting of crystalline PCL (soft segments) is observed in the curves of WPU/CN nanocomposite at approximately 42 °C that is not observed for neat WPU, indicating the crystalline and amorphous nature of the WPU/CN nanocomposites and the WPU matrix, respectively. This is consistent with observations made from WAXD that supported the presence of a crystalline structure in the WPU/CN nanocomposites. This melting temperature value is close to the melting temperature reported for neat WPU based on PCL having a molecular weight over 2000 which show a partially crystalline structure.<sup>47</sup> Moreover, the heat of fusion ( $\Delta H_m$ ) and the corresponding degree of crystallinity of WPU/CN nanocomposites significantly increase from 0.6 to 9.8 Jg<sup>-1</sup> and from 0.66% to 11.39%, respectively, with the increase of CN content from 2 to 10 wt-%. In contrast to the case of WPU filled with unmodified CNs this melting peak was not observed<sup>35</sup> which confirms, as stated previously, that the crystallization was not nucleated at the surface of unmodified CNs, but only induced by grafted WPU-chains on the surface of CNs. Compared to the value of  $\Delta H_m$  of PCL diol (around 71 Jg<sup>-1</sup>, not shown), the much lower  $\Delta H_m$  of WPU/CN nanocomposites is an indication of the restricted crystallization. This can be explained by the fact that  $T_g$  of the hard segment is higher than the crystallization temperature (about 40 °C) of the PCL soft segments and the crystallization of PCL segments is restricted by the hard segments in glassy state. For the same reason, no crystallization is observed for the pure WPU.<sup>47</sup>

### Mechanical properties of WPU/CN nanocomposites

The storage modulus ( $E'$ ) and loss modulus ( $E''$ ) of the WPU/CN nanocomposite films with different CN loading as a function of temperature are shown in Fig. 9. At a very low temperature (< –40 °C), neat WPU exists in the glassy state and the molecular motions are largely restricted to vibration and short-range rotation. As the temperature increased, the storage modulus decreased slightly. A rapid decrease of the storage modulus is observed as the temperature becomes higher than –35 °C, which corresponds to the primary relaxation process ( $\alpha$ ), namely the glass-rubber transition of WPU. In the rubbery region, the value of the storage modulus keeps decreasing with temperature due to the irreversible polymeric chain flow arising from the elastomeric nature of WPU. In contrast to the neat WPU, the storage modulus curves of all WPU/CN nanocomposite films displayed a typical behavior of partially crystalline polymers with three distinctive zones. At low temperature (below –40 °C) which corresponds to the glassy state, the modulus decreased slightly with temperature. At approximately –35 °C, a transition that appears as a sharp drop in the storage modulus is observed, which is also due to the main relaxation process. At a temperature range between –35 to approximately 50 °C, the amorphous,

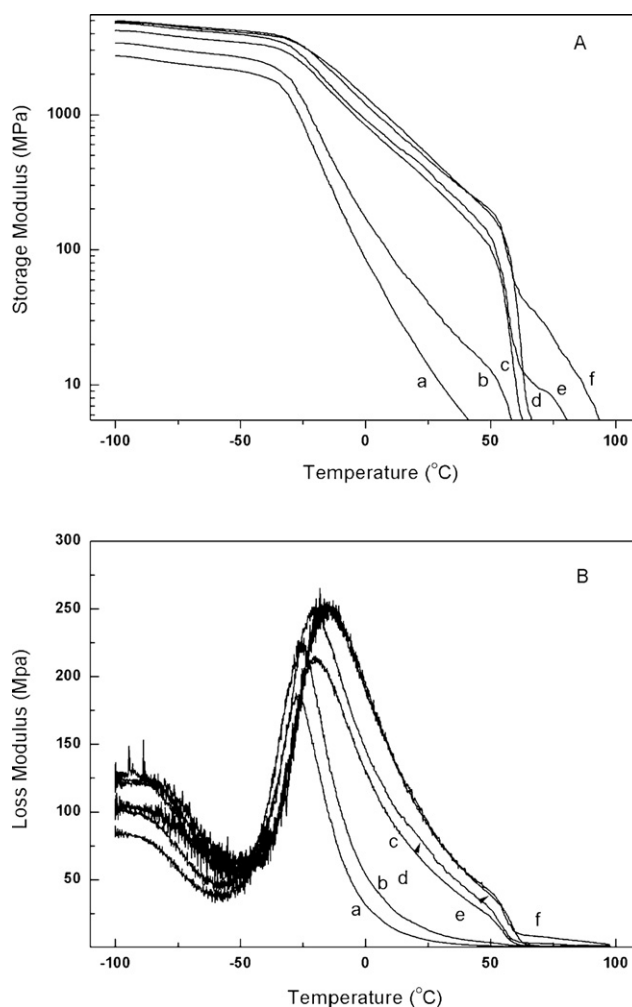


**Fig. 9** DMA results of the WPU/CN nanocomposite films with different CNs loading: (a) WPU, (b) WPU/CN-2, (c) WPU/CN-4, (d) WPU/CN-6, (e) WPU/CN-8, (f) WPU/CN-10.

rubbery, and crystalline domains coexist and the storage tensile modulus decreased due to the progressive flow of amorphous WPU chains and also the melting of the crystalline part of the matrix. At higher temperatures (above 50 °C) the modulus dropped sharply and unrecoverable deformations occurred due to the complete melting of the crystalline zones of the WPU matrix. This significant difference confirms again the presence of a crystalline structure within the WPU/CN nanocomposites.

In addition, the value of the modulus of the nanocomposite films increased significantly upon filler addition as compared to the neat WPU. This enhanced rigidity can be related to both the presence and increase of the crystalline part in WPU/CN nanocomposites as shown by DSC and WAXD measurements and to the reinforcing effect of the CNs as is already well-known. In addition, as already demonstrated, the thermal stability of the WPU/CN nanocomposite films increased. All these observations lead to the conclusion that strong adhesion forces exist between the reinforcing phase and the matrix, arising from efficient dispersion of the CNs and efficient stress transfer at the interface *via* the co-continuous phase created in large part to the co-crystallization of the grafted WPU chains on the surface of CNs and the WPU matrix.

From the loss modulus curves (Fig. 9B), an  $\alpha$  transition peak can be easily identified and the temperature at the peak is assigned as the glass transition temperature ( $T_g$ ) of the soft segments of WPU matrix. The  $T_g$  shifts to higher temperature with the incorporation of CNs in the WPU matrix because of their good confinement, which is in good agreement with all previous results. Furthermore, the  $T_g$  peaks of the WPU/CN nanocomposites are broadened due to the motion of polymer chains at the WPU-CN interface area.<sup>48</sup> The higher storage modulus and higher  $T_g$  as well as the broadened  $\alpha$  transition peak of the WPU/CN nanocomposites indicate again that a strong adhesion exists between the reinforcing fillers of CN and the matrix of WPU.

The mechanical behavior that resulted from large deformations of the films based on neat WPU and the nanocomposites reinforced with CNs was investigated by tensile tests at room temperature. Fig. 10 shows the stress-strain curves of these films, and two characteristic regions of deformation behavior can be observed. At low strains, the stress increases linearly with an increase of strain, and the Young's modulus was calculated from the initial slope in this elastic region. At higher strain, the deformation feature of the nanocomposite films greatly depends on the loading level of CNs. When the loading level of CNs is lower than 8 wt-%, the stress regularly increases with the strain, increasing up to the ultimate fracture of the films. However, the nanocomposite films with 10 wt-% of CNs, which have the highest degree of crystallinity (11.73%), display behavior typical

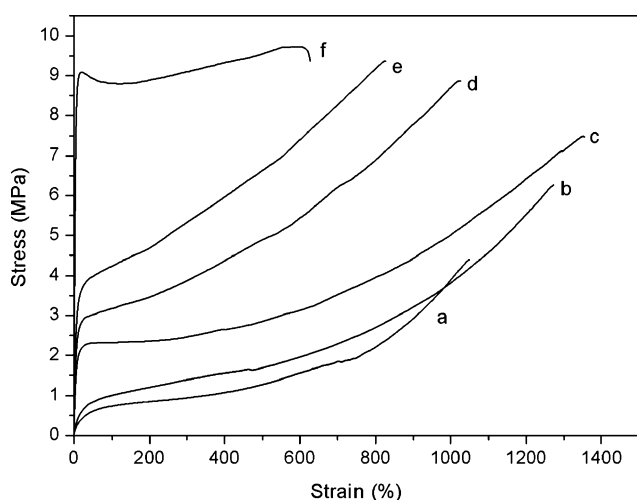


**Fig. 10** Stress-strain curves for the WPU/CN nanocomposite films with different CNs loading: (a) WPU, (b) WPU/CN-2, (c) WPU/CN-4, (d) WPU/CN-6, (e) WPU/CN-8, (f) WPU/CN-10.

**Table 3** Mechanical properties of WPU and the WPU/CN nanocomposites obtained from tensile tests: Young's modulus ( $E$ ), Tensile strength ( $\sigma_B$ ), and Elongation at break ( $\epsilon_B$ )

Sample	$E$ (MPa)	$\sigma_B$ (MPa)	$\epsilon_B$ (%)
WPU	$1.7 \pm 0.2$	$4.4 \pm 0.2$	$1049.5 \pm 30.6$
WPU/CN-2	$5.4 \pm 1.3$	$6.3 \pm 1.2$	$1273.3 \pm 36.4$
WPU/CN-4	$22.5 \pm 2.3$	$7.5 \pm 0.8$	$1355.2 \pm 60.3$
WPU/CN-6	$41.4 \pm 1.8$	$8.9 \pm 1.1$	$1027.2 \pm 25.9$
WPU/CN-8	$55.6 \pm 3.6$	$9.4 \pm 0.5$	$827.1 \pm 30.4$
WPU/CN-10	$107.4 \pm 6.2$	$9.7 \pm 0.6$	$626.6 \pm 13.2$

of rigid and tough thermoplastics with a necking down, similar to the behavior of polycaprolactone based films.<sup>49</sup> When the nanocomposite films were prepared by blending CNs from flax fibers and WPU in water, they did not show any necking phenomenon even when the loading level of fillers reached 30 wt-%. This was due to the amorphous structure of the WPU matrix and the absence of any crystalline structure when loaded with unmodified CNs. Therefore, it can be concluded easily that the presence of the crystalline regions in the WPU/CN nanocomposites prepared play an important role in converting the nanocomposites from elastomer-like materials to thermoplastic-like materials.

The Young's modulus, tensile strength, and elongation at break were determined from the curves, and the results are presented in Table 3. Because of its amorphous nature, the WPU shows a nonlinear elastic behavior, possesses a low tensile strength of 4.4 MPa, a low Young's modulus of 1.7 MPa, and a high elongation at break of about 1049%. The CNs content has a profound effect on the tensile properties. It is evident that even a small amount of CNs can largely improve the tensile properties. For the WPU/CN nanocomposite containing 2 wt-% CNs, Young's modulus and tensile strength are about 217% and 43%, respectively, higher than those for the pure WPU film. In the nanocomposites, generally, the Young's modulus and tensile strength are significantly increased as compared with pure WPU. The Young's modulus increases with the CNs loading level, reaching the highest value of 107.4 MPa at 10 wt-% of CNs, approximately 60-fold higher than for the matrix, while the improvement was four times less (15-fold) when the same amount of unmodified CNs were used.<sup>35</sup> The largest improvement for the tensile strength reached 9.7 MPa for the nanocomposites loaded with 10 wt-% of CNs. In contrast to conventional filled polymer systems, the increase of strength has a price: it is achieved only at the expense of ductility. The values of elongation at break of the WPU/CN nanocomposites increase with an increase of CNs content in the range of 0–4 wt-%,

**Table 2** DSC results for WPU and WPU/CN nanocomposites with various CNs content

Samples	$T_g$ (mid, °C)	$\Delta C_p$ ( $Jg^{-1}K^{-1}$ )	$T_m$ (°C)	$\Delta H_m$ ( $Jg^{-1}$ )	$\chi_c$ (%)
WPU	-47.97	0.32	—	—	0
WPU/CN-2	-44.98	0.30	42.51	0.60	0.66
WPU/CN-4	-45.25	0.34	41.76	1.83	2.06
WPU/CN-6	-44.58	0.28	42.56	4.92	5.66
WPU/CN-8	-45.27	0.25	41.66	5.19	6.10
WPU/CN-10	-43.47	0.29	42.63	9.48	11.39

reaching a maximum value of 1355% for the WPU/CN-4. When the CN loading level is higher than 6 wt-%, the elongation at break of the nanocomposites decreases slightly. Generally, the results from the tensile tests indicate that the mechanical properties of the WPU/CN nanocomposites are greatly improved in comparison to neat WPU. All of these results can be explained by the reinforcement of the WPU matrix by homogeneously dispersed CNs fillers and the ensuing strong interaction between CNs and the WPU matrix through a co-continuous phase created in large part to the co-crystallization of grafted-WPU chains and those from the matrix. This co-continuous phase acts as network fulcrum point to transfer local stress evenly to all other WPU chains, which in a general sense enhances the mechanical properties of the nanocomposites.

## Conclusions

A series of WPU/CNs nanocomposites were prepared *via* one-pot polymerization, surface grafting, and processing. Some of the pre-synthesized WPU chains were successfully grafted to CNs through the reaction between the isocyanates of the WPU pre-polymers and hydroxyls of CNs. These grafted-WPU chains were able to form a crystalline structure on the surface of CNs, and thus induce the crystallization of the matrix which created a co-continuous phase. As a result, very good dispersion and strong interfacial adhesion between CNs and WPU were obtained. Therefore, the incorporation of CNs in WPU resulted in a significant improvement in the thermal stability and the mechanical properties.

## Acknowledgements

We would like to acknowledge all the members of the Laboratory of Soft Materials & Green Chemistry at NC State University (NC SU) who continuously provide a collegial and supportive environment to help us conduct our work. We would like to acknowledge Miss Michelle Casper in Department of Materials Science and Engineering (NC SU) for WARD measurements and USDA Grant No. 2006-38411-17035 for financial support.

## References

- 1 B. Kim, J. Seo and H. Jeong, *Eur. Polym. J.*, 2003, **39**, 85–91.
- 2 H. Kuan, C. Ma, W. Chuang and H. Su, *J. Polym. Sci., Part B: Polym. Phys.*, 2005, **43**, 1–12.
- 3 H. Lee, J. Hwang and H. Liu, *J. Polym. Sci., Part A: Polym. Chem.*, 2006, **44**, 5801–5807.
- 4 H. Lee and L. Lin, *Macromolecules*, 2006, **39**, 6133–6141.
- 5 C. Zhao and W. Zhang, *Eur. Polym. J.*, 2008, **44**, 1988–1995.
- 6 H. Kuan, C. Ma, W. Chang, S. Yuen, H. Wu and T. Lee, *Compos. Sci. Technol.*, 2005, **65**, 1703–1710.
- 7 J. Kwon and H. Kim, *J. Polym. Sci., Part A: Polym. Chem.*, 2005, **43**, 3973–3985.
- 8 J. Kwon and H. Kim, *J. Appl. Polym. Sci.*, 2005, **96**, 595–604.
- 9 M. A. S. Azizi Samir, F. Alloin and A. Dufresne, *Biomacromolecules*, 2005, **6**, 612–626.
- 10 P. Podsiadlo, S. Choi, B. Shim, J. Lee, M. Cusihy and N. Kotov, *Biomacromolecules*, 2005, **6**, 2914–2918.
- 11 W. Helbert, J. Y. Cavaille and A. Dufresne, *Polym. Compos.*, 1996, **17**, 604–611.

- 12 A. Sturcova, G. R. Davies and S. J. Eichhorn, *Biomacromolecules*, 2005, **6**, 1055–1061.
- 13 F. Favier, H. Chanzy and J. Y. Cavaille, *Macromolecules*, 1995, **28**, 6365–6367.
- 14 D. Fengel and G. Wegner, *Wood: Chemistry, Ultrastructure, Reactions*, Walter de Gruyter, New York, 1984.
- 15 A. P. Mathew and A. Dufresne, *Biomacromolecules*, 2002, **3**, 609–617.
- 16 P. Terech, L. Chazeau and J. Y. Cavaille, *Macromolecules*, 1999, **32**, 1872–1875.
- 17 J. R. Capadona, K. Shanmuganathan, D. J. Tyler, S. J. Rowan and C. Weder, *Science*, 2008, **319**, 1370–1374.
- 18 J. R. Capadona, O. Van Den Berg, L. A. Capadona, M. Schroeter, S. J. Rohan, D. J. Tyler and C. Weder, *Nat. Nanotechnol.*, 2007, **2**, 765–769.
- 19 S. J. Hanley, J. Giasson, J. F. Revol and G.D.G., *Polymer*, 1992, **33**, 4639–4642.
- 20 J. F. Revol, *Carbohydr. Polym.*, 1982, **2**, 123–134.
- 21 M. Grunert and W. T. Winter, *J. Polym. Environ.*, 2002, **10**, 27–30.
- 22 C. Tokoh, K. Takabe, M. Fujita and H. Saiki, *Cellulose*, 1998, **5**, 249–261.
- 23 Y. Lu, L. Weng and X. Cao, *Carbohydr. Polym.*, 2006, **63**, 198–204.
- 24 Y. Habibi and A. Dufresne, *Biomacromolecules*, 2008, **9**, 1974–1980.
- 25 Y. Habibi, A.-L. Goffin, N. Schiltz, E. Duquesne, P. Dubois and A. Dufresne, *J. Mater. Chem.*, 2008, **18**, 5002–5010.
- 26 J. Araki, M. Wada, S. Kuga and T. Okano, *Colloids Surf., A*, 1998, **142**, 75–82.
- 27 S. Beck-Candanedo, M. Roman and D. G. Gray, *Biomacromolecules*, 2005, **6**, 1048–1054.
- 28 M. Castonguay, J. T. Koberstein, Z. Zhang and G. Laroche, in *Biomedical Applications of Polyurethanes*, ed. P. Vermette, H. J. Griesser, G. Laroche and R. Guidoin, Lands Bioscience, Georgetown, Texas USA, 2001, p. 284.
- 29 M. Modesti and A. Lorenzetti, *Eur. Polym. J.*, 2001, **37**, 949–954.
- 30 W. C. Chan and S. A. Chen, *Polymer*, 1993, **34**, 1265–1270.
- 31 M. Dreja, K. Heine, B. Tieke and G. J. Junkers, *J. Colloid Interface Sci.*, 1997, **191**, 131.
- 32 C. K. Kim and B. K. Kim, *J. Appl. Polym. Sci.*, 1991, **43**, 2295–2301.
- 33 Z. W. Wicks, D. A. Wicks and J. W. Rosthauser, *Prog. Org. Coat.*, 2002, **44**, 161–183.
- 34 H. Kuan, M. Ma, W. Chang, S. Yuen, H. Wu and T. Lee, *Compos. Sci. Technol.*, 2005, **65**, 1703–1710.
- 35 X. Cao, H. Dong and C. M. Li, *Biomacromolecules*, 2007, **8**, 899–904.
- 36 G. Chen, M. Wei, J. Chen, J. Huang, A. Dufresne and R. P. Chang, *Polymer*, 2008, **49**, 1860–1870.
- 37 M. Labet, W. Thielemans and A. Dufresne, *Biomacromolecules*, 2007, **8**, 2916–2927.
- 38 J. F. Watts and J. Wolstenholme, *An Introduction to Surface Analysis by XPS and AES*, John Wiley & Sons Ltd, Chichester 2003.
- 39 V. Crescenzi, G. Manzini, C.G. and C. Borri, *Eur. Polym. J.*, 1972, **8**, 449–463.
- 40 A. Dufresne, *Can. J. Chem.*, 2008, **86**, 484–494.
- 41 W. Thielemans, M. N. Belgacem and A. Dufresne, *Langmuir*, 2006, **22**, 4804–4810.
- 42 Y. Nishiyama, P. Langan and H. Chanzy, *J. Am. Chem. Soc.*, 2002, **124**, 9074–9082.
- 43 J. Sugiyama, R. Vuong and H. Chanzy, *Macromolecules*, 1991, **24**, 4168–4175.
- 44 R. G. J. C. Heijkants, R. V. van Calck, T. G. van Tienen, J. H. de Groot, P. Buma, A. J. Pennings, R. P. H. Veth and A. J. Schouten, *Biomaterials*, 2005, **26**, 4219–4228.
- 45 A. R. Sarasam, R. K. Krishnaswamy and V. Madihally, *Biomacromolecules*, 2006, **7**, 1131–1138.
- 46 M. Roman and W. T. Winter, *Biomacromolecules*, 2004, **5**, 1671–1677.
- 47 P. Ping, W. Wang, X. Chen and X. Jing, *Biomacromolecules*, 2005, **6**, 587–592.
- 48 K. J. Yao, M. Song, D. J. Hourston and D. Z. Luo, *Polymer*, 2002, **43**, 1017–1020.
- 49 H. J. Lee, H. W. Choi, K. J. Kim and S. C. Lee, *Chem. Mater.*, 2006, **18**, 5111–5118.